MELT REFINING, SOLIDIFICATION, AND DOWNSTREAM PROCESSING TO MITIGATE CASTING DEFECTS

Simulation Analysis of Influence of Argon Gas Injection Hole Position on Flow Field in Steel Ladle

ZHU TAN,[1] YUE YU,[1] XIAODONG DENG,[1] and JIANLI LI ●[1,2,3,4]

1.—The State Key Laboratory of Refractories and Metallurgy, Wuhan University of Science and Technology, Wuhan 430081, China. 2.—Hubei Provincial Key Laboratory for New Processes of Ironmaking and Steelmaking, Wuhan University of Science and Technology, Wuhan 430081, China. 3.—Key Laboratory for Ferrous Metallurgy and Resources Utilization of Ministry of Education, Wuhan University of Science and Technology, Wuhan 430081, China. 4.—e-mail: jli@wust.edu.cn

Analysis of the effect of argon bottom blowing on stirring and refining in a ladle was carried out using numerical simulation based on a 250-ton ladle. The flow field inside the ladle was calculated for different bottom-blowing hole angles and radial positions, and the influence of the distance between the bottom-blowing holes and refining effect was investigated. The results indicate that as the bottom-blowing flow rate increases, the rate of change in the dead zone inside the ladle gradually decreases and drops sharply at 950 L/min. When the angle between the two bottom-blowing holes increases from 90° to 180 ° under the same bottom-blowing flow rate, the maximum velocity at the steel-liquid interface decreases and the average flow velocity of the steel liquid increases. When the bottom-blowing aperture is at a position of $r/R = 0.5$, the stirring effect of the steel liquid is good, and when $r/R = 0.67$ is arranged. When the spacing ratio is constant, the relative position changes, and the bottom-blowing effect hardly changes. When the spacing ratio increases from 0.707 to 1, the mixing effect of the steel liquid improves, and the refining effect of the steel-liquid interface decreases.

INTRODUCTION

With the increasing demand for quality steel in the market, strict control of steel composition has become crucial.[1–3] The slag steel reaction in the secondary refining process is a key aspect of producing clean steel, and bottom-blowing argon technology has been widely used in the refining process because of its simplicity, feasibility, and economy. A reasonable bottom-blowing process has good effects on removing inclusions, homogenizing temperature, and composition in steel. It is necessary to choose appropriate gas flow rates and bottom-blowing hole arrangements for different refining purposes.[4–6]

Krishnapisharody[7] pointed out that many models have not been fully tested because of the difficulty in measuring specific parameters of inclusions even in water models. The purpose of the current work is to use multiphase fluid dynamics calculations to simulate the movement inside the ladle, obtain stirring efficiency and refining effect. Previous studies[8–10] simulated the process of slag entering the molten steel and found the relationship between inclusion content and mass transfer rates at different interfaces. It was found that gas flow rate had the most significant effect on the formation rate of slag droplets, while the viscosity of slag had almost no effect on the formation of slag droplets. Therefore, this study fixed the viscosity of slag, taking the nozzle angle and radial position as variables. In terms of the number of nozzles, the desulfurization efficiency of dual hole blowing is higher than that of single hole eccentric blowing, because dual hole blowing can generate more bubbles, increase the contact area between oxidant and slag and molten steel, and promote the reaction.[11] In addition, dual hole injection can also improve gas distribution, making the dissolved oxygen concentration in the entire molten steel more uniform.[12] Villela Aguilar

et al.[13–15] found that the angle between the bottom-blowing holes is the most relevant variable in reducing mixing time, and a good asymmetric configuration can reduce the mixing time of the secondary refining furnace.

At present, research has divided the angle and radial distance into two separate variables to explore their effects, and the radial distance and angle together determine the linear distance between the positions of the two bottom-blowing holes. This article establishes a ladle model and explores the influence of different bottom-blowing flow rates on mixing and refining effects from the angle and radial position of the blowing holes and the ratio of the distance between the two bottom-blowing holes. This provides a reference for designing a reasonable ladle bottom-blowing system.

EXPERIMENTAL SETUP

Mathematical Model

Geometric Similarity

Research has shown that a suitable similarity ratio can reduce the error of simulation calculations. In this experiment, a similarity ratio was established using a 250-ton ladle from a steel plant as a prototype, λ = 1:6. The mathematical model has the following specific parameters shown in Table I.

Bottom-blowing hole position: In this study, dual hole spraying was used, with bottom-blowing hole angles arranged at 90°, 120°, and 180° and radial positions at distances of 151.5 mm (0.5R) and 202 mm (0.67R) from the center of the circle, as shown in Fig. 1a.

Physical Similarity

The main driving forces for internal flow in the system are bubble initial velocity and buoyancy. Therefore, it is necessary to ensure that the corrected Froude number of both factors is equal to guarantee dynamic similarity between the prototype and mathematical model

$$F_r^{'} = \frac{\rho_g d^2 v^2 \left(\frac{\pi}{4}\right)}{\rho_l g D^2 H \left(\frac{\pi}{4}\right)} \# \tag{1}$$

where $F_r^{'}$ represents the corrected Froude number; ρ_g and ρ_l are the densities of gas and liquid, respectively. v represents the gas flow rate at the bottom; g is the gravitational acceleration, which is taken as 9.80 m/s^2 in this case; d represents the

diameter of the porous plug. D represents the diameter of the melt. H represents the depth of the melt.

It can be concluded

$$v^{'} = \lambda^{-0.5} v \# \tag{2}$$

where λ represents the similarity ratio, and $v^{'}$ denotes the simulated model's bottom-blowing gas velocity.

Bottom-blowing velocity is represented as

$$v = \frac{4Q}{n\pi d^2} \# \tag{3}$$

where Q represents the bottom-blowing gas flow rate, and n denotes the number of nozzles.

Assumptions

Due to the complexity of the physical and chemical reactions that occur inside the bottom-blown steelmaking furnace, factors such as the size of argon bubbles, drag coefficients, and accumulation of slag layers cannot be completely simulated. However, various simulation methods can still provide guidance for on-site operations.

The basic assumptions for this experiment are:

(1) The liquid phase is assumed to be the continuous phase, while the gas phase is assumed to be the discrete phase. Initially, the melt is full of liquid phase.
(2) The gas-liquid two-phase region satisfies the full buoyancy model, where the driving force is the buoyancy of the gas bubbles, and the density of the liquid phase in the two-phase region remains constant.
(3) The surface of the slag phase is treated as a free surface.
(4) The liquid phase is assumed to be an incompressible fluid, and the flow of the liquid phase inside the melt is steady state.
(5) The influence of temperature and concentration fields on the flow field is neglected.

Boundary Conditions

Melt surface: The molten liquid and slag are in contact with each other on the surface of the melt, and the pressure on the slag surface is atmospheric pressure. The gas phase enters the atmosphere from this surface, while the liquid phase is not allowed to leave the system.

Table I. Model parameters (mm)

	Bottom radius	Top radius	Ladle height	Depth of molten steel	Thickness of slag layer
Noumenon	1817	1956	4130	3500	50
Model	303	326	688	583	8.3

Simulation Analysis of Influence of Argon Gas Injection Hole Position on Flow Field in Steel Ladle
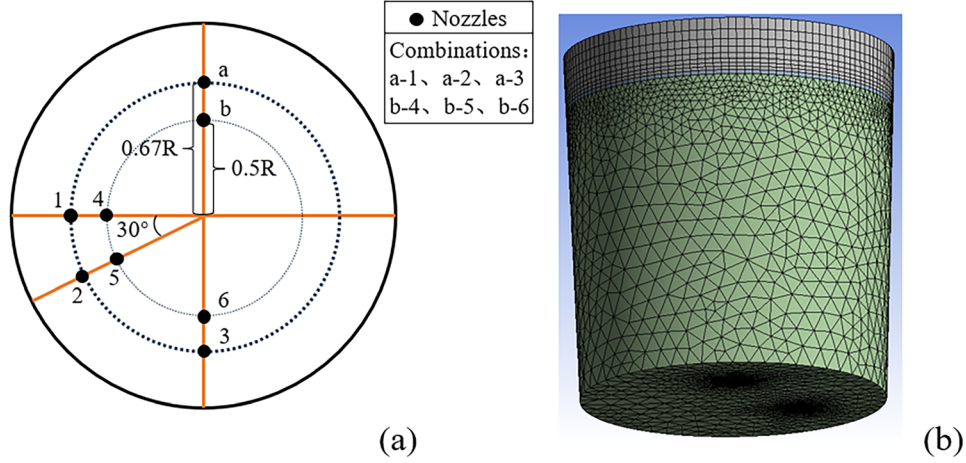

Fig. 1. Schematic diagram of nozzle position (a) and grid division situation (b).

Table II. Bottom-blowing flow rate and velocity

Prototype bottom-blowing flow rate (L/min)	Prototype bottom-blowing velocity (m/s)	Model bottom-blowing velocity (m/s)
500	0.287	0.117
800	0.459	0.187
900	0.516	0.211
950	0.5453	0.223
1000	0.574	0.234
1050	0.603	0.246
1200	0.688	0.281

Wall: All wall surfaces are impermeable, and the flow parameters are zero. The transport process of momentum and scalar near the wall is determined by the wall function.

Inlet: The bottom nozzle is a velocity inlet boundary, and only gas enters, and the bottom-blowing flow rate and velocity are shown in Table II.

Basic Equations

The flow of molten steel in the ladle under argon bottom blowing is a complex turbulent flow process, characterized by irregularity, three dimensionality, diffusivity, and dissipation. The equations that describe the flow of molten liquid in the ladle include the continuity equation, and momentum equation (Navier–Stokes equation), with RNG $k-\varepsilon$ model for turbulence modeling and VOF (volume of fluid) model for multiphase flow modeling, calculated in conjunction with standard wall models. The governing equations are as follows.[16]

Continuity equation

$$\nabla \cdot (\rho \boldsymbol{V}) = 0 \# \tag{4}$$

Momentum equation

$$\rho \frac{\partial \overrightarrow{u}}{\partial t} + \rho \overrightarrow{u} \cdot \nabla \overrightarrow{u} = -\nabla \overrightarrow{p} + \rho \overrightarrow{g} + \nabla \cdot \mu (\nabla \overrightarrow{u} + \nabla^T \overrightarrow{u}) + \overrightarrow{f} \# \tag{5}$$

where ρ is density, μ is effective viscosity, $\overrightarrow{u}$ is velocity vector, p is pressure, and $\overrightarrow{f}$ is volume force.

Phase equation

$$\frac{\partial \alpha}{\partial t} + \overrightarrow{u} \cdot \nabla \alpha = 0 \# \tag{6}$$

k equation

$$\frac{\partial}{\partial t}(\rho \mathrm{k}) + \frac{\partial}{\partial x_i}(\rho k u_i) = \frac{\partial}{\partial x_j}\left[\left(\mu + \frac{\mu_t}{\delta_k}\right)\frac{\partial k}{\partial x_j}\right] + G_k + G_b - \rho \varepsilon - Y_m + S_k \# \tag{7}$$

ε equation

$$\frac{\partial}{\partial t}(\rho \varepsilon) + \frac{\partial}{\partial x_i}(\rho k u_i) = \frac{\partial}{\partial x_j}\left[\alpha_\varepsilon u_{\mathrm{eff}}\frac{\partial \varepsilon}{\partial x_j}\right] + c_{1\varepsilon}\frac{\varepsilon}{k}(G_k + G_{3\varepsilon}G_b) - C_{2\varepsilon}\rho\frac{\varepsilon^2}{k} - R_\varepsilon + S_\varepsilon \# \tag{8}$$

where Y_m represents the effect of wave expansion on turbulent dissipation rate; μ_i represents the time-averaged velocity of turbulent flow; k represents the turbulent fluctuation kinetic energy; ε represents the turbulent fluctuation kinetic energy dissipation

rate; G_k represents the turbulence energy generated by the velocity gradient of laminar flow; G_b represents the turbulence energy generated by buoyancy.

Grid Partitioning and Solution Methods

The calculation area grid of the ladle is shown in Fig. 1b, using an orthogonal Cartesian coordinate system to divide tetrahedral and hexahedral grids throughout the entire area. To ensure calculation accuracy and save calculation time, a denser grid division format is used in the entrance area and slag layer area, while a relatively sparse grid division format is used in other areas, with a grid size of 350,000. The solving algorithm adopts SIMPLE transient calculation with a time step of 0.05 s to ensure that the residual converges to 10^{-4} at each step. By detecting the velocity at a certain point in the ladle and waiting for the flow inside the ladle to stabilize, the average value of 20 s is calculated to evaluate the average level of the solution.

RESULTS AND DISCUSSION

Liquid Steel Flow Field

After the gas is injected into the bottom-blowing holes, the upward movement of the gas drives the stirring of the steel liquid. As the bottom-blowing progresses, the velocity and direction distribution of the double-hole section. The velocity flow gradually diverges, and eddy currents are formed on both sides, which become more intense when the velocity flow reaches the slag-steel interface. In the gap between the rising bubbles, the intensity of the eddy current decreases, and this process repeats. Figure 2 shows the cloud map of the slag layer and the cross-section of the ladle at this time. The trace near the ladle wall in the upper left corner of Fig. 2d indicates that when the gas bubble flow hits the

slag layer, some of it turns into horizontal movement, then moves downward when it hits the ladle wall, and due to the influence of buoyancy, the velocity decreases to zero and begins to flow upward, forming an eddy current.

At various flow rates, the velocity distribution of the steel liquid on the cross-section shows a similar trend. The higher velocity regions are concentrated above the nozzles, and the different gas contents cause density differences, generating buoyancy to drive the flow of the steel liquid. The area with a velocity < 0.01 m/s is defined as the stirring dead zone. Figure 3a calculates the dead zone ratio and average velocity of the steel liquid at different bottom-blowing flow rates for bottom-blowing hole angles of 120°, 90°, and 180°, obtaining their stirring effects.

Table III shows the dead zone ratio (Δ dead zone ratio/Δ flow rate) at various bottom-blowing flow rates for a 120° angle and $r/R = 0.67$. As the bottom-blowing flow rate increases, the dead zone ratio gradually decreases, but the rate of decrease significantly slows down after reaching 950 L/min. Between 500 and 1000 L/min, the dead zone ratio decreases significantly, and from 1000 to 1200 L/min, the rate of reduction decreases. The overall trend of the dead zone ratio for angles of 90° and 180° is similar to that for the 120° angle condition. When the two nozzles are at a 180° angle, the dead zone area is lower than that at a 90° angle at low flow rates. However, at higher flow rates, the dead zone ratio is slightly higher than that at a 90° angle. This indicates that the refining effect and mixing effect do not follow the same trend and degree of change with increasing flow rate for different angle arrangements. This is consistent with the results of Conejo's research.[17] Higher average flow velocity corresponds to the overall mixing efficiency of the
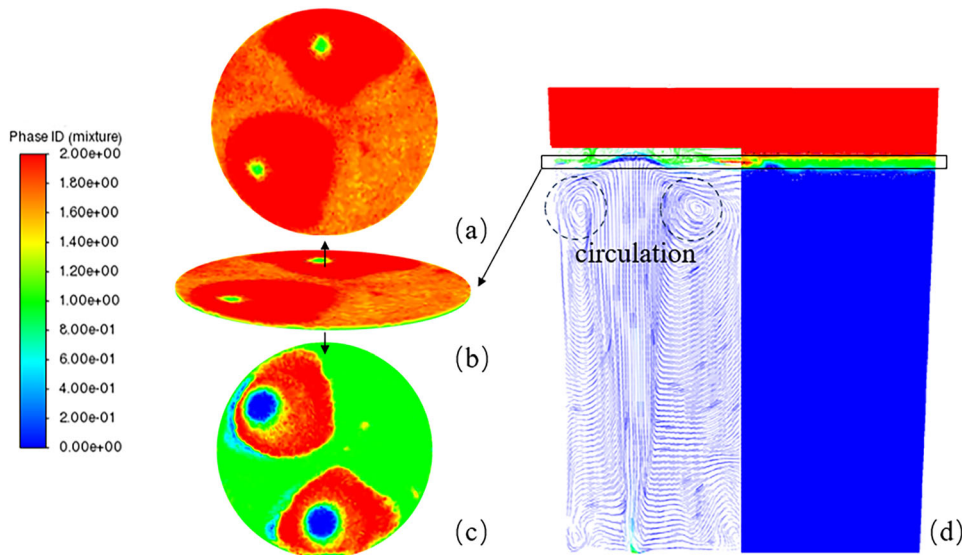

Fig. 2. Top view cloud diagram of slag layer top (a) and main view (b) and bottom cloud diagram of slag layer (c) and overlay diagram of cross-section cloud diagram trace (d) where steel liquid phase is blue, slag phase is green, and gas phase is red (Color figure online).
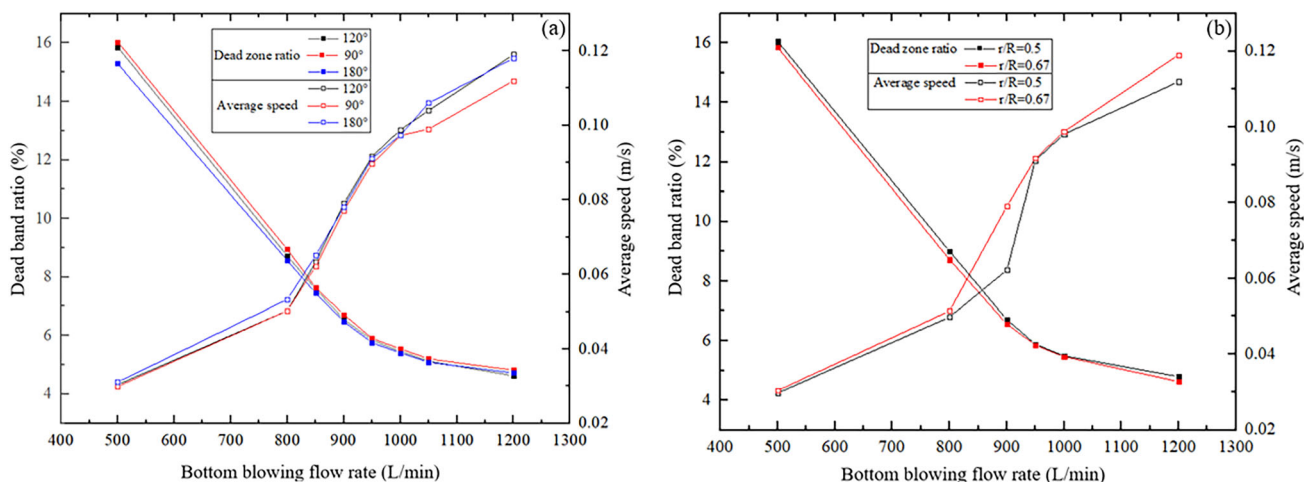
Fig. 3. The relationship between bottom-blowing flow rate and dead zone ratio/average velocity of molten steel at (a) different bottom-blowing angles and (b) different radial positions.

Table III. The proportion and rate of change of dead zones at each bottom-blowing flow rate at an angle of 120 ° and r/R = 0.67

Blowing flow rate (L/min)	Dead zone ratio (%)	Change rate
500	15.85	–
800	8.72	0.0238
850	7.58	0.0228
900	6.56	0.0208
950	5.79	0.0154
1000	5.42	0.0074
1050	5.13	0.0058
1200	4.62	0.0034

ladle. The higher the average flow velocity, the greater the stirring velocity is. Higher velocity is more likely to generate turbulence, produce more eddies, and increase the disorder of fluid motion, thereby achieving more thorough mixing. Figure 3b shows the relationship between the bottom-blowing flow rate and the dead zone ratio as well as the average steel liquid velocity at different radial positions of the nozzle for a 120° angle. The average velocity at r/R = 0.5 is lower than that at r/R = 0.67.

Flow Field Near the Slag Layer

Figure 4 shows the change of the top of the slag layer with the injection process: in the initial stage, the slag layer protrudes, and slag holes appear above one side of the nozzle. Afterwards, the slag holes gradually become larger, and after reaching an extreme value, the protrusion above the other nozzle also breaks through the slag layer and begins to appear. At the same time, the area of the first slag eye begins to decrease until the newly appeared slag eye area reaches its extreme value, and the first slag eye gradually increases again. Finally, both slag eye areas reach their extreme value and are similar in size.

The maximum flow rate at the slag-steel interface can display refining efficiency within a certain range.[18] As the bottom-blowing flow rate increases, the maximum flow velocity at the slag-steel interface also increases, the slag steel contact is more complete, and the refining efficiency is also better. However, if the flow rate is too high, the area of slag hole formation will also become larger, which may cause secondary pollution to the steel liquid. The velocity dense areas are all located above the nozzle and gradually approach the steel ladle wall. The maximum velocity of the interface under various conditions is calculated as shown in Fig. 5. When the two nozzles adopt an angle distribution of 90° and 120°, the velocity approaches 0 at the edge far from the two pores, but the maximum velocity is higher than the angle of 180°. When the two nozzles are arranged at an angle of 120°, they are on the same side. Compared to the 180° opposite distribution of the two nozzles, the distance between the two airflow columns is reduced, and the impact on the flow field between them is increased. By increasing the bottom-blowing flow rate, the stirring intensity is increased, while also reducing the impact on the slag layer. Compared to the distribution at a 90°
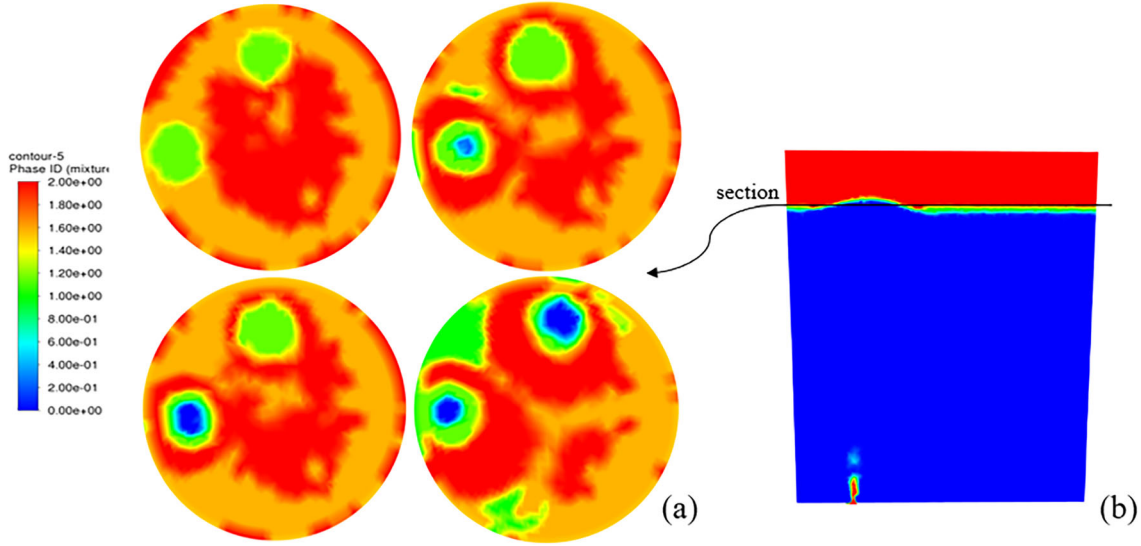
Fig. 4. Cloud map of slag layer changes (a) and section position (b) (90°, 900 mL/min, r/R = 0.67).
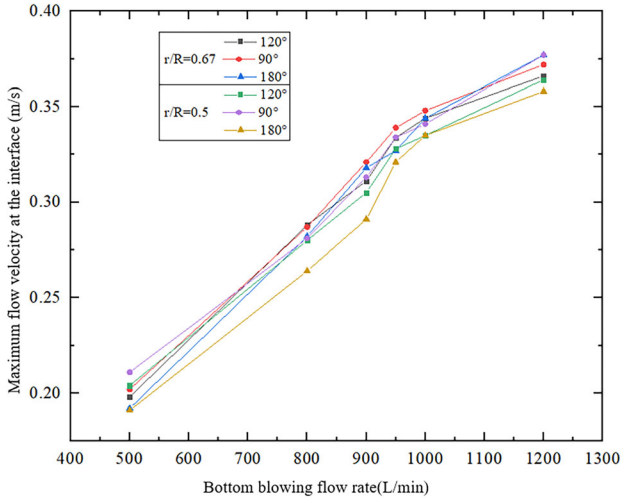

Fig. 5. Bottom-blowing flow rate and maximum velocity at slag-steel interface.

angle, it reduces the energy dissipation caused by the influence of convection and has a higher utilization rate of momentum; Ramasetti's research[19] has similar results.

The radial position of the two nozzles also has a significant impact on the maximum flow velocity at the steel-slag interface. When $r/R = 0.5$ and the included angle is 90°, the distance between the two nozzles is the closest, and the impact between them is significant. The joint impact results in a maximum interface velocity of 0.377 m/s. Although the refining strength is high, the velocity is relatively concentrated, and the proportion of weak areas is large. The average velocity of the entire steel liquid is relatively low, indicating low mixing efficiency. Moreover, excessive interface speed can also lead to excessive slag hole area, causing secondary pollution. When $r/R = 0.5$ and the included angle is 180°,

the distribution of the two nozzles is uniform, and the kinetic energy consumption is minimal. Therefore, a higher average velocity of the molten steel and a minimum maximum velocity at the interface are obtained. When $r/R = 0.67$ and the included angle is 180°, the kinetic energy consumption is also small, and there is a higher average velocity of the steel liquid. However, due to being relatively close to the steel ladle wall, some bubbles and steel liquid flow rebound after hitting the steel ladle wall and then return to the upward bubbles and steel liquid flow.

The Influence of Nozzle Spacing Ratio

In the current study, the effects of angle and radial distance were investigated as two variables on mixing and refining. When the bottom-blowing flow rate was sufficient, both the angle and radial position had a significant impact on mixing and refining. The radial distance and angle jointly determined the straight-line distance between the two bottom-blowing nozzles. To better analyze the effect of the bottom-blowing position on blowing, a dimensionless parameter, the bottom-blowing spacing ratio, was defined.

$$\delta = d/R \qquad (9)$$

where d represents the straight-line distance between the two bottom-blowing nozzles in meters, and R is the radius of the bottom of the ladle in meters. A smaller δ indicates a shorter distance between the two nozzles. Table IV below shows the spacing ratios for various combinations of nozzle positions as set in Fig 1. Combining Figs. 3 and 5 shows that as the spacing ratio gradually increases, the average velocity of the steel liquid inside the ladle increases, the dead zone ratio decreases, and the maximum velocity at the interface decreases.

Table IV. Spacing ratio of each combination

Combinations	δ
a-1	0.943
a-2	1.155
a-3	1.333
b-4	0.707
b-5	0.866
b-6	1

To verify the above trends, the effectiveness of the nozzle arrangement was evaluated by fixing the c-nozzle as the bottom-blowing nozzle and following the layout as shown in Fig. 6. To ensure basic bottom-blowing efficiency, cases where the two nozzles are distributed within the same quadrant of the circle were excluded. Additionally, to reduce erosion of the ladle wall, cases where the radial position r/R is > 0.75 were also excluded.

Figure 7a shows the values of dead zone ratio and average velocity at different bottom-blowing flow rates when $\delta = 0.707$. When δ is constant, the relative position change has little effect on the dead zone ratio and average velocity of the steel liquid. This is because under the three arrangements of $\delta 1$, the mutual influence between the two bottom-blowing nozzles is almost the same, and the dissipation of kinetic energy by the ladle wall is also small. For Fig. 7b, when $\delta = 0.886$, the dead zone ratio in the ladle changes with the relative position of the two bottom-blowing nozzles, with $\delta 21$ and $\delta 22$ varying, while $\delta 22$ and $\delta 23$ remain almost the same. This is because when $\delta 21$ is arranged, the two nozzles are concentrated on one side and close to the ladle wall. After colliding with the ladle wall, some of the bubbles flow back and collide with the bottom-blown bubble flow, resulting in energy loss. However, the three arrangements of $\delta 1$ and the arrangements of $\delta 22$ and $\delta 23$ have less energy loss because the two bottom-blowing nozzles are far from the ladle wall and distributed more evenly, resulting in little change in dead zone ratio and average velocity. The trend for $\delta 31$ and $\delta 32$ in Fig. 7c is similar. This indicates that the main factors affecting mixing and homogenization efficiency are the spacing between the two bottom-blowing nozzles and the distance between the bottom-blowing nozzle and the ladle wall. When the spacing between the two bottom-blowing nozzles is appropriate and far from the ladle wall, the change in relative position has little effect on the blowing efficiency.

Figure 8 shows the distribution of maximum velocity at the slag-steel interface under various arrangements. When the bottom-blowing spacing ratio remains constant, the maximum velocity at the interface is almost unaffected by the change in relative position of the bottom-blowing nozzles. As the bottom-blowing spacing increases, the
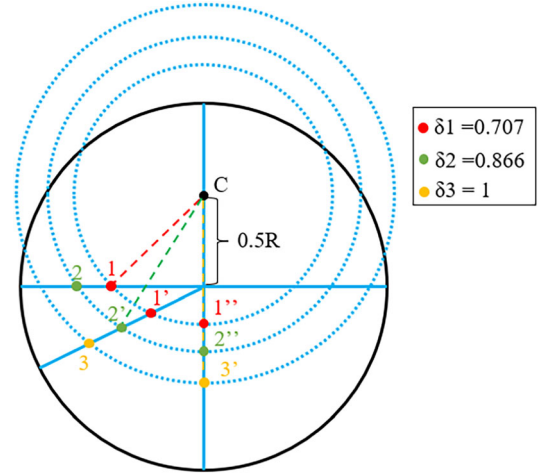

Fig. 6. Arrangement of bottom-blowing holes at different δ.

probability of interaction and fusion of the rising bubble flows from the two bottom-blowing nozzles decreases, resulting in a gradual decrease in the maximum interface velocity. This coincides with the plans[20,21] of adopting a moderate radial position of 0.5–0.67 and an angle of 120°–180°.

CONCLUSION

The influence of the angle, radial position, and spacing ratio of the bottom-blowing holes on the bottom-blowing effect was studied through numerical simulation of the process of bottom-blowing argon in a ladle. The following conclusions were drawn:

1. When the two nozzles are arranged at a 120° angle, compared to the distribution of the two nozzles at a 180° angle, the maximum velocity at the interface is larger, indicating better refining efficiency. Compared to the distribution with a 90° angle, the utilization rate of kinetic energy is higher, indicating better mixing and homogenization efficiency. When the two nozzles are located radially at $r/R = 0.5$, there is a higher interface velocity, which is more conducive to refining. At the radial position of $r/R = 0.67$, there is a larger average steel liquid flow velocity, which is conducive to mixing and homogenization. Within the appropriate range of bottom-blowing flow rate, when the angle or radial position increases, the average velocity of the steel liquid increases and the maximum interface velocity decreases.
2. Within the experimental range, when the spacing ratio of the two bottom-blowing nozzles is appropriate, the change in relative position has little effect on the blowing efficiency. As the bottom-blowing spacing ratio increases, the average velocity of the steel liquid increases, and the maximum interface velocity decreases, resulting in better mixing and homogenization
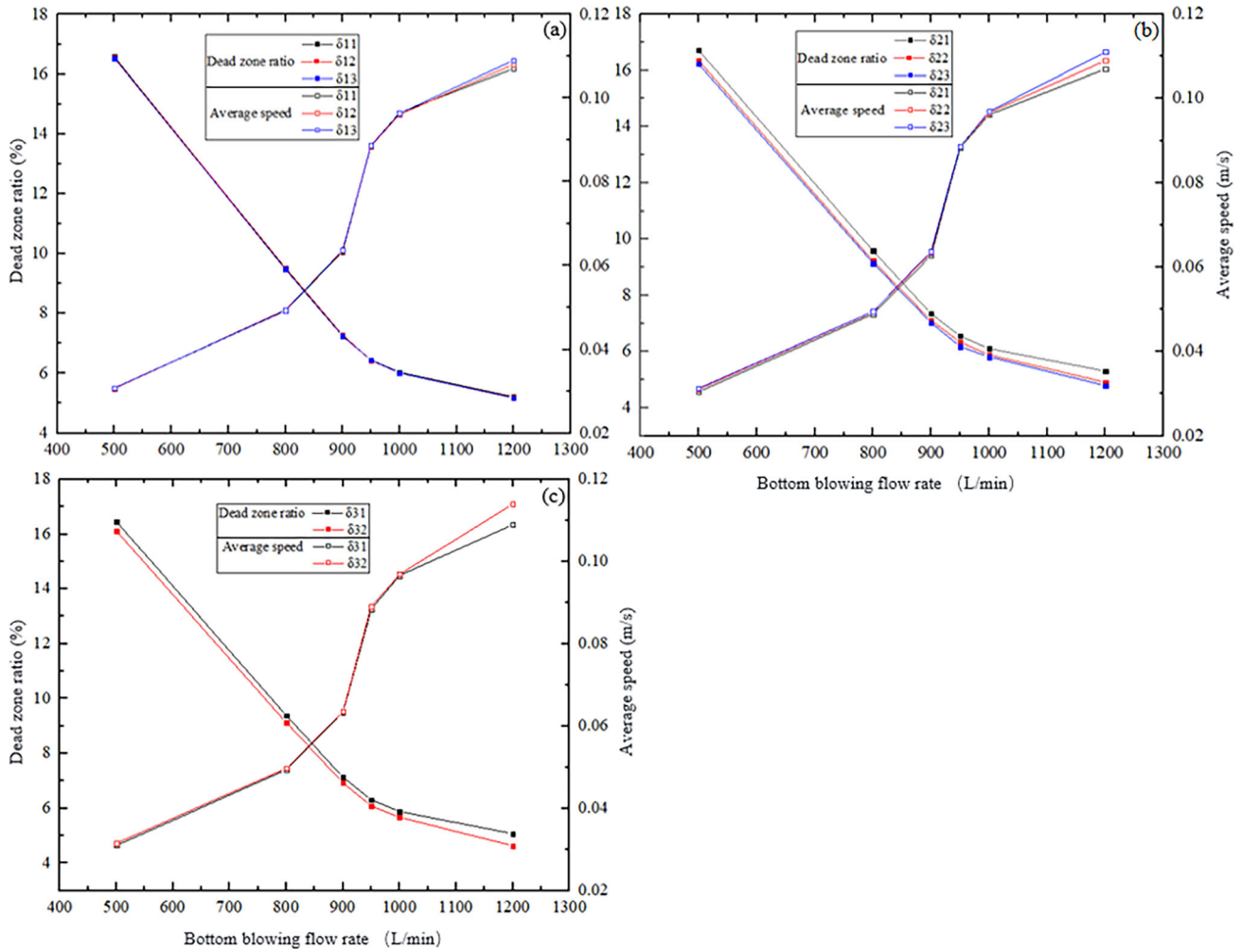
Fig. 7. Dead zone ratio and average velocity under different bottom-blowing flow rates at (a) $\delta 1$; (b) $\delta 2$; (c) $\delta 3$.
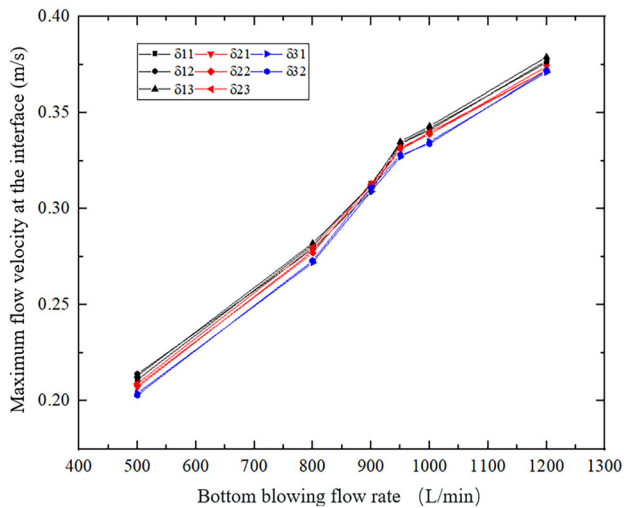

Fig. 8. Bottom-blowing flow rate and maximum velocity at slag-steel interface.

effects, but reduced refining efficiency. The recommended value of δ is in the range of 1–1.155.

CONFLICT INTEREST

On behalf of all authors, the corresponding author states that there is no conflict of interest.

REFERENCES

1. B. Yuan and J. Liu, *J. Zeng. Met.* 12, 434 (2022).
2. K. Lambrighs, I. Verpoest, B. Verlinden, et al., *Procedia Eng.* 2(1), 173 (2010).
3. C. Chen, Z. Jiang, and Y. Li, *ISIJ Int.* 60, 617 (2020).

4. A. Huang, H. Gu, M. Zhang, et al., *Metall. Mater. Trans. B* 44(3), 744 (2013).
5. H. Liu, Z. Qi, and M. Xu, *Steel Res. Int.* 82(4), 440 (2011).
6. L.F. Zhang and B.G. Thomas, *Metall. Mater. Trans. B* 37(5), 733 (2006).
7. G. Irons, A. Senguttuvan, and K. Krishnapisharody, *Trans. Iron Steel Inst. Jpn.* 55(1), 1 (2015).
8. A. Senguttuvan and G.A. Irons, *ISIJ Int.* 57(11), 1962 (2017).
9. Q.N. Hoang, M.A. Ramírez, and A.N. Conejo, *JOM* 70, 2109 (2018).
10. D.H. Zhang, M.G. Shen, and C. Wu, *J. Iron. Steel Res. Int.* 22, 48 (2015).
11. U. Singh, R. Anapagaddi, and S. Mangal, *Metall. Mater. Trans. B* 47(3), 1804 (2016).
12. Q. Cao and L. Nastac, *Metall. Mater. Trans. B* 49B(3), 1388 (2018).
13. Q. Li and P.C. Pistorius, *JOM* 73, 2888 (2021).
14. X. Cui, Y. Xue, D. Zhao, et al., *High Temp. Mater. Process. (Lond.)* 40(1), 471 (2021).
15. A.S. Gómez, A.N. Conejo, and V.R. Zenit, *J. Appl. Fluid Mech.* 11(1), 11 (2018).
16. S. Patankar, *Numerical Heat Transfer and Fluid Flow* (Taylor & Francis, Milton Park, 1980).
17. K. Niu, W. Feng, and A.N. Conejo, *Metall. Mater. Trans. B* 54(4), 2066 (2023).
18. S. Yokoya, S. Takagi, M. Iguchi, et al., *ISIJ Int.* 40(6), 572 (2000).
19. E.K. Ramasetti, V.V. Visuri, P. Sulasalmi, et al., *Steel Res. Int.* 90, 1800365 (2018).
20. H.Y. Tang, X.C. Guo, and G.H. Wu, *ISIJ Int.* 56(12), 2161 (2016).
21. H.Y. Tang, G.W. Liu, et al., *Ironmak. Steelmak.* 46, 405 (2019).